ACS APPLIED MATERIALS & INTERFACES

Research Article

www.acsami.org

Aptamer-Modified Micro/Nanostructured Surfaces: Efficient Capture of Ramos Cells in Serum Environment

Yanyun Wang, Feng Zhou, Xiaoli Liu,* Lin Yuan, Dan Li, Yanwei Wang, and Hong Chen*

Jiangsu Key Laboratory of Advanced Functional Polymer Design and Application, Department of Polymer Science and Engineering, College of Chemistry, Chemical Engineering and Materials Science, Soochow University, 199 Ren'ai Road, Suzhou, 215123, P. R. China

Supporting Information

ABSTRACT: For potential applications in the isolation and enrichment of circulating tumor cells (CTCs), we have developed gold nanoparticle layers (GNPLs) of different roughness modified with TD05 aptamers (GNPL-APT). In serum-free binary cell mixtures containing Ramos cancer cells and CEM cells, the density of Ramos cells adherent to highly rough GNPL-APT was 19 times that of CEM cells. However, in serum-containing conditions, the specificity of GNPL-APT for Ramos cells was much reduced. To improve Ramos specificity in the presence of serum, we attached the TD05 aptamer to the layers via poly(oligo(ethylene glycol) methacrylate) (POEGMA) as an antifouling spacer (GNPL-POEGMA-APT). In serum-containing environment GNPL-POEGMA-APT showed an enhanced selectivity for Ramos cells, which increased with increasing surface roughness. The results of this study indicate that surfaces combining appropriate chemical composition and micro/nano roughness structures may be useful for cell separation, including the isolation of cancer cells for diagnosis.

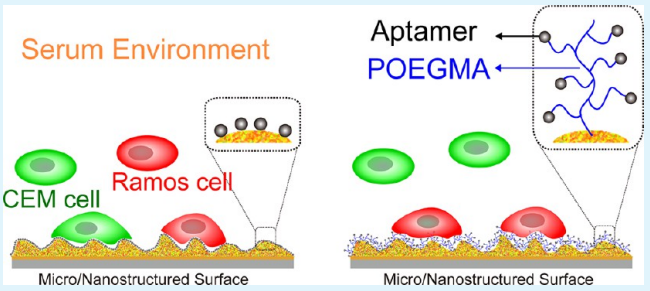

KEYWORDS: *aptamer, surface roughness, cancer cells, selective capture, serum*

INTRODUCTION

Early diagnosis and treatment play a vital role in improving survival rates in cancer patients.[1] Circulating tumor cells (CTCs) are considered to be crucial in the progression of cancer,[2,3] and the detection of CTCs may be a useful approach in diagnosis, treatment, and prognosis.[4] However, CTCs are present in very small numbers in blood: one CTC cell per 1×10^5 to 1×10^7 normal blood cells.[4] Therefore CTC enrichment is a prerequisite for the development of CTC analysis as a cancer diagnostic tool.[4] Over the past few decades, much work has been done to develop reliable methods for CTC enrichment and identification. At the present time, the main methods are filtration, density gradient centrifugation,[5] and immunomagnetic enrichment.[6] Many methods such as ISET (isolation by size of epithelial tumor cells),[7] density gradient and OncoQuick[5,8] are based on cell size and thus are of low specificity. The immunomagnetic method identifies CTCs on the basis of epithelial markers such as EpCAM and CKs.[4,9,10] Although this method enhances specificity to some extent, it suffers from other limitations: for example, CKs also exist in some activated leukocytes;[4] and expression the EpCAM marker appears to decline in tumor cells undergoing the epithelial to mesenchymal transition, where CTC cells lose epithelial characteristics such as the expression of specific markers.[9−11]

In recent years, researchers have noted that micro/nanostructures on surfaces can significantly enhance cell-surface interactions including cell adhesion;[12,13] this effect can be exploited for the enrichment and separation of CTCs. In addition to microstructure, surface chemistry also plays a role in cell adhesion. For example, aptamers that may be considered as nucleic acid forms of traditional antibodies[14−16] can be designed to have specific affinity for cells. They are easily produced in vitro and have good stability and high target specificity. Moreover, aptamers have been designed as efficient diagnostic probes for tumors both in vitro and in vivo.[17,18] Thus using appropriate surface topography and aptamer modification, surfaces may be designed to capture specific cells. For example, in a single cell environment, Chen et al. found that the density of CCRF-CEM cells on aptamer-modified silicon nanowire arrays was about 2 orders of magnitude greater than that on aptamer-modified planar silicon surface.[19] In binary cell mixtures, Zhou et al. found that target Molt-3 cells were enriched up to 94% on an aptamer modified surface in a microfluidic channel system.[20] Wan et al. found that aptamer functionalized, nanotextured polydimethylsiloxane (PDMS) enriched a 1:1 mixture of fibroblasts and target human glioblastoma (hGBM) cells to 1:5.5 by selective adhesion.[21]

However, in a more realistic setting, e.g. human blood, many other cells will compete with target cells. Moreover, proteins

Received: February 4, 2013
Accepted: March 29, 2013
Published: March 29, 2013

   dx.doi.org/10.1021/am400469g | ACS Appl. Mater. Interfaces 2013, 5, 3816−3823

Scheme 1. Process of Surface Modification

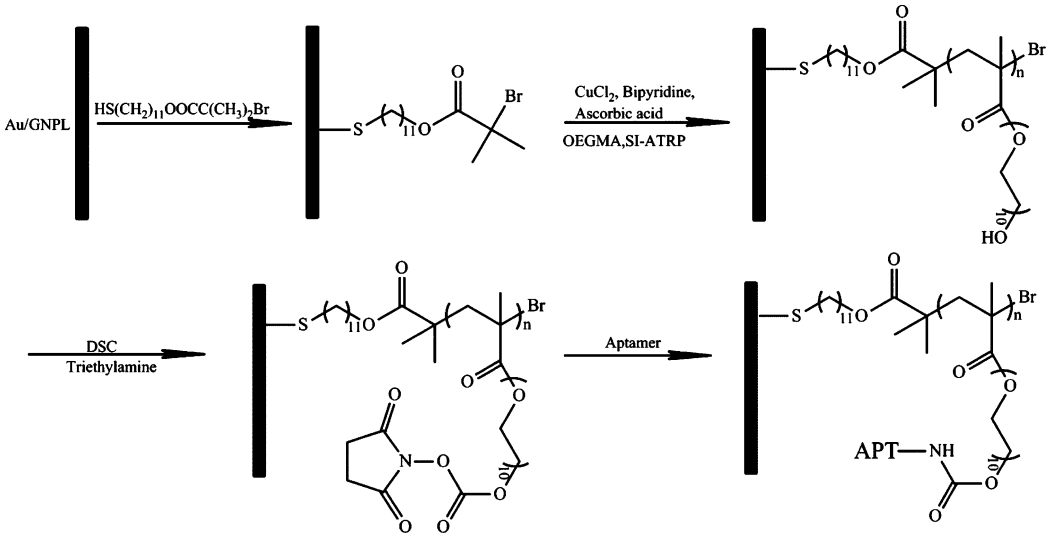

may adsorb nonspecifically and thus interfere with the interactions of specific receptors on the cell surface and surface immobilized aptamers. The research mentioned above gave data only for single cell or binary cell systems. In this work, we prepared GNPLs with controlled surface morphology by a simple and convenient method; we also investigated POEGMA as an antifouling spacer for the aptamer. The B leukemia CTC cell, Ramos cell, was selected as a target to study the selective capture capability of cell specific aptamer-modified GNPLs of varying surface roughness in serum-free and serum-containing cell culture conditions.

EXPERIMENTAL SECTION

Materials. Silicon wafers 0.53 mm thick, polished on both sides, were coated with a chromium adhesion layer followed by a layer of gold (approximately 100 nm) and diced into 0.5 cm × 0.5 cm pieces. CellTracker Green CMFDA (Invitrogen, C2925) and CellTracker Orange CMTMR (Invitrogen, C2927) were from Invitrogen. Hydrogen tetrachloroaurate hydrate ($HAuCl_4 \cdot 4H_2O$), glucose, glutaraldehyde (2.5%), cupric chloride, N,N′-disuccinimidyl carbonate (DSC), acetonitrile, and absolute methanol were from Sinopharm Chemical Reagent Co., Ltd. (Shanghai, China). Potassium hydrogen carbonate was from Shanghai Zhanyun Chemical Co., Ltd. (Shanghai, China). Bipyridine, oligo(ethylene glycol) methacrylate (OEGMA) (n = 10, M_w = 526 g/mol) were from Sigma. Mercaptoethylamine was from Aladdin. TD05 aptamer, with high specific affinity for Ramos cells, was from Shanghai Sangon Biotechnology Co., Ltd. (Shanghai, China). The sequence of the TD05 aptamer is: 5′-CAC CGG GAG GAT AGT TCG GTG GCT GTT CAG GGT CTC CTC CCG GTG TTT TT-$(CH_2)_6$-HS/NH_2-3′. The CEM (CL1014, T cell line, human ALL) cell line and Ramos cells (CL1012, B-cell, human Burkitt's lymphoma) were from Abgent Biotechnology Co., Ltd.

Fabrication of GNPLs on Gold Films. Details of the fabrication of GNPLs on gold films have been reported previously.[22] First, the gold surface was modified with mercaptoethylamine by a self-assembling method to introduce amino groups. Cleaned gold films were immersed in 20 mmol/L mercaptoethylamine in ethanol overnight at room temperature. The gold films were then rinsed with absolute ethanol and deionized water to remove physically adsorbed molecules, and dried under nitrogen. Finally, the films were placed in the wells of a 48-well plate, and 150, 300, or 500 μL plating solution (12 mM $HAuCl_4 \cdot 4H_2O$, 0.5 M $KHCO_3$, and 25 mM glucose) was added to each well. Incubation at 35 °C for 3 h gave gold nanoparticle layers designated GNPL1, GNPL2, and GNPL3, respectively, for an increasing volume of the plating solution. The GNPLs were rinsed three times with deionized water and dried under nitrogen. With increasing volume of plating solution, the surface roughness of the layers increased due to the increasing density of nanoparticles.[22] The root-mean-square surface roughness, R_q, measured with a roughmeter (SJ-210, Mitutoyo, Japan), was ∼51 nm, ∼85 nm, and ∼211 nm, respectively. Details of the surface roughness and morphology characterization can be found in our previous work.[22]

Modification of GNPLs with Aptamers. 2.5 OD TD05 APT (for single-stranded DNA, 1 OD ≈ 33 μg) (3′ end modified with a mercapto group) was dissolved in 2 mL phosphate buffered saline (PBS) (2.25 nmol/L). Smooth gold and nanoparticle surfaces were treated with the aptamer solution at room temperature for 3 h and then washed with PBS to remove excess aptamer. The samples (Au-APT and GNPL-APT) were then dried under N_2.

Modification of GNPLs with Aptamers via POEGMA Spacer. The procedures for the preparation of POEGMA-modified smooth gold and nanoparticle surfaces have been reported previously.[22] POEGMA-modified Au surfaces and GNPLs (Au-POEGMA and GNPL-POEGMA) were treated with DSC in dry acetonitrile at room temperature for about 5 h. The DSC modified surfaces (Au-POEGMA-NHS and GNPL-POEGMA-NHS) were then washed with acetonitrile and dried under nitrogen. The samples were immersed in aptamer solution (3′ end modified with amino group) for 3 h at 37 °C to give the APT-modified Au-POEGMA (Au-POEGMA-APT) and APT-modified GNPL-POEGMA (GNPL-POEGMA-APT) surfaces. The procedure is shown in Scheme 1.

Surface Characterization. Static water contact angles were measured with a SL200C optical contact angle meter (USA Kino Industry Co., Ltd.) using the sessile drop method at room temperature. The thickness of the surface layers was measured using an α-SE spectroscopic ellipsometer (J.A. Woollam Co., Inc.). The chemical composition of the surfaces was determined by XPS (ESCALAB MK II X-ray photoelectron spectrometer, VG Scientific).

Cell Culture and Cell Capture Assay. The CEM and Ramos cells were cultured in DMEM medium supplemented with 10% fetal bovine serum (FBS), 2 mM glutamine, 100 U/ml penicillin and 10 mg/mL streptomycin at 37 °C with 5% CO_2. The unmodified and APT modified samples were placed in the wells of 48-well tissue culture plates, and treated with 75% ethanol for 20 min. The samples were then rinsed three times with sterile ultrapure water. Cells were harvested by centrifugation and trypanblue staining showed that cell viability was >95%. The cell suspension was washed with sterilized phosphate buffered saline (PBS, pH 7.4) and the cells were collected by centrifugation (5 min, 100 g). The Ramos cells were treated with orange fluorescent dye (CellTracker Orange CMTMR) in PBS (0.5 μmol/L) at 37 °C for 30 min in a constant-temperature incubator.

They were collected by centrifugation after staining, and then washed twice with prewarmed PBS at 37 °C to remove excess dyes and collected by centrifugation (5 min, 100 g). CEM cells were treated with green fluorescent dye (CellTracker Green CMFDA) in PBS (0.5 μmol/L). The staining procedure was the same as for the Ramos cells. The CEM and Ramos cells were dispersed separately in DMEM medium and then mixed in equal numbers. The unmodified and modified gold films were placed into the wells of 48-well plates, and then 1 mL of a cell suspension (5.0×10^4 cells/mL) was loaded. In one group the medium contained 10% (v/v) serum and the other group was serum free. After incubation for 1.5 to 2 h at 37 °C (5% CO_2) the samples were washed twice with PBS at 37 °C to remove nonattached cells, then fixed with 2.5% glutaraldehyde for 20 min and dehydrated using a series of ethanol solutions of increasing concentration (30−100%).

The cells were then observed by light microscopy (BX51, Olympus) for cell counting (magnification: × 40). The density of adhered cells was determined using Image J (National Institutes of Health; http://rsbweb.nih.gov/ij/; version: 1.67) and Image-Pro Plus 6.0.

MTT Assay. Cell viability of the captured Ramos cells on the surface was assessed using MTT assay. First, the medium was replaced by 200 μL fresh medium. Then 20 μL of 5 mg/mL MTT was added and the wells were incubated for 4 h. After that, the medium was aspirated, and the MTT-formazan generated by live cells was dissolved in 220 μL of DMSO. Finally, 200 μL of the solution from each well was transferred into the adjacent empty wells, and absorbance values at 490 nm for MTT were measured using a microplate reader (Thermo Fisher Scientific Inc.).

RESULTS AND DISCUSSION

Surface Characterization. *XPS.* Table 1 shows quantitative elemental composition data for GNPL3 surfaces before and after aptamer modification. For the unmodified GNPL3 surface, gold, sulfur, carbon, and nitrogen were detected, reflecting surface modification by mercaptoethylamine. Oxygen, attributed to unavoidable contamination of the GNPL surfaces during analysis,[23] were also detected. After the self-assembly of aptamer (GNPL3-APT), the appearance of additional phosphorus element with an atomic concentration of 2.92% indicated successful immobilization of aptamer.

Table 1. Atomic Concentrations of Unmodified and APT Modified GNPL3 from XPS (90° take-off angle)

surface	C (%)	O (%)	N (%)	Au (%)	S (%)	P (%)
GNPL3	46.40	19.36	5.68	26.58	1.98	
GNPL3-APT	42.44	14.04	5.78	31.82	2.94	2.92
GNPL3-POEGMA	66.80	32.34	0.70	0.16		
GNPL3-POEGMA-NHS	68.46	30.22	1.02	0.28		
GNPL3-POEGMA-APT	67.26	30.78	1.08	0.12		0.78

The C/O ratio for GNPL3-POEGMA was determined to be 2.1, equal to the value of 2.1 expected for POEGMA.[24] Also the ellipsometric thickness of the POEGMA layer on GNPL3-POEGMA was 47.7 ± 0.1 nm, confirming that POEGMA was successfully grafted on the GNPL surface. After DSC modification (GNPL3-POEGMA-NHS), the nitrogen concentration increased. The additional phosphorus seen after aptamer treatment indicated successful attachment of the aptamer to the GNPL3-POEGMA-NHS surface.

Water Contact Angles. As shown in Figure 1a, the water contact angle decreased with increasing surface roughness: from 64° on the smooth gold surface to 15° on GNPL3. Because single-stranded DNA has high content of phosphate, hydroxyl and other hydrophilic groups, the contact angles were reduced significantly after aptamer modification.[21] For example, the angle of smooth gold was reduced from ∼64° to ∼18°. Moreover, the water contact angles of the aptamer-modified GNPL surfaces were all less than 10° (GNPL3-APT less than 5°) indicating superhydrophilic character in agreement with the Wenzel model.[25]

For the GNPL-POEGMA surfaces the water contact angles again decreased with increasing roughness (Figure 1(b)): from ∼54° (Au-POEGMA) to ∼29° (GNPL3-POEGMA). After aptamer modification the contact angles decreased significantly, and for the GNPL2-POEGMA-APT and GNPL3-POEGMA-APT surfaces were <10°, indicating superhydrophilicity. As seen in Figure 1b the contact angles showed a strong dependence on surface roughness.

Cell Culture and Cell Capture Assay. *Ramos Cell Capture on GNPL-APT Surfaces.* Cell adhesion in single cell solutions was first investigated on the unmodified GNPL surfaces. In both serum-free and serum-containing conditions, large numbers of both Ramos and CEM cells were seen to

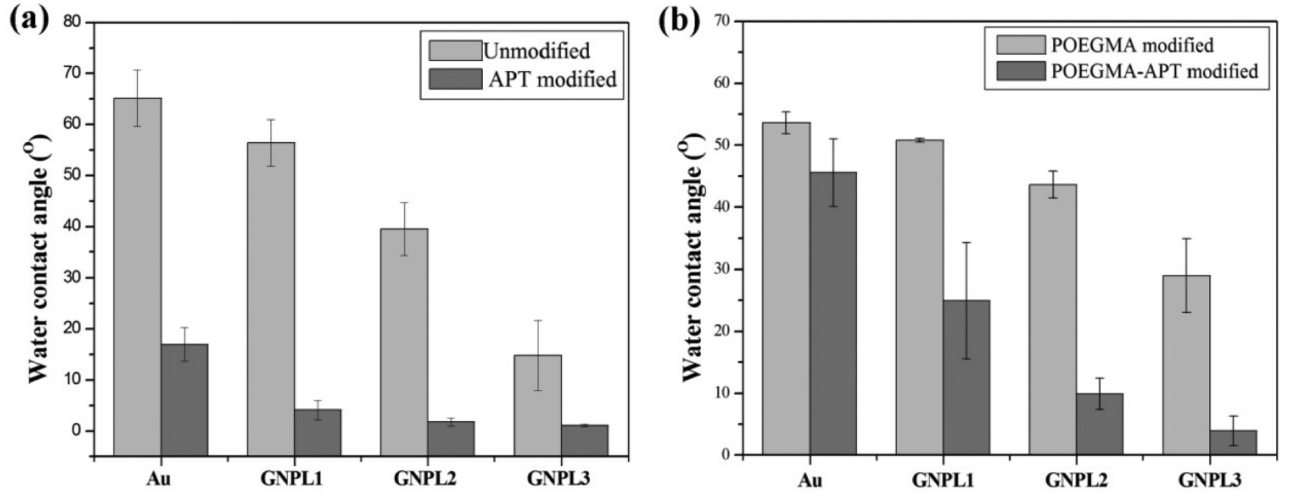

Figure 1. Water contact angles. (a) Au and GNPL(1 to 3) before and after the modification with TD05 aptamer (mean ± SD, n = 3); (b) Au-POEGMA and GNPL(1 to 3)-POEGMA before and after the modification with TD05 aptamer (mean ± SD, n = 3).

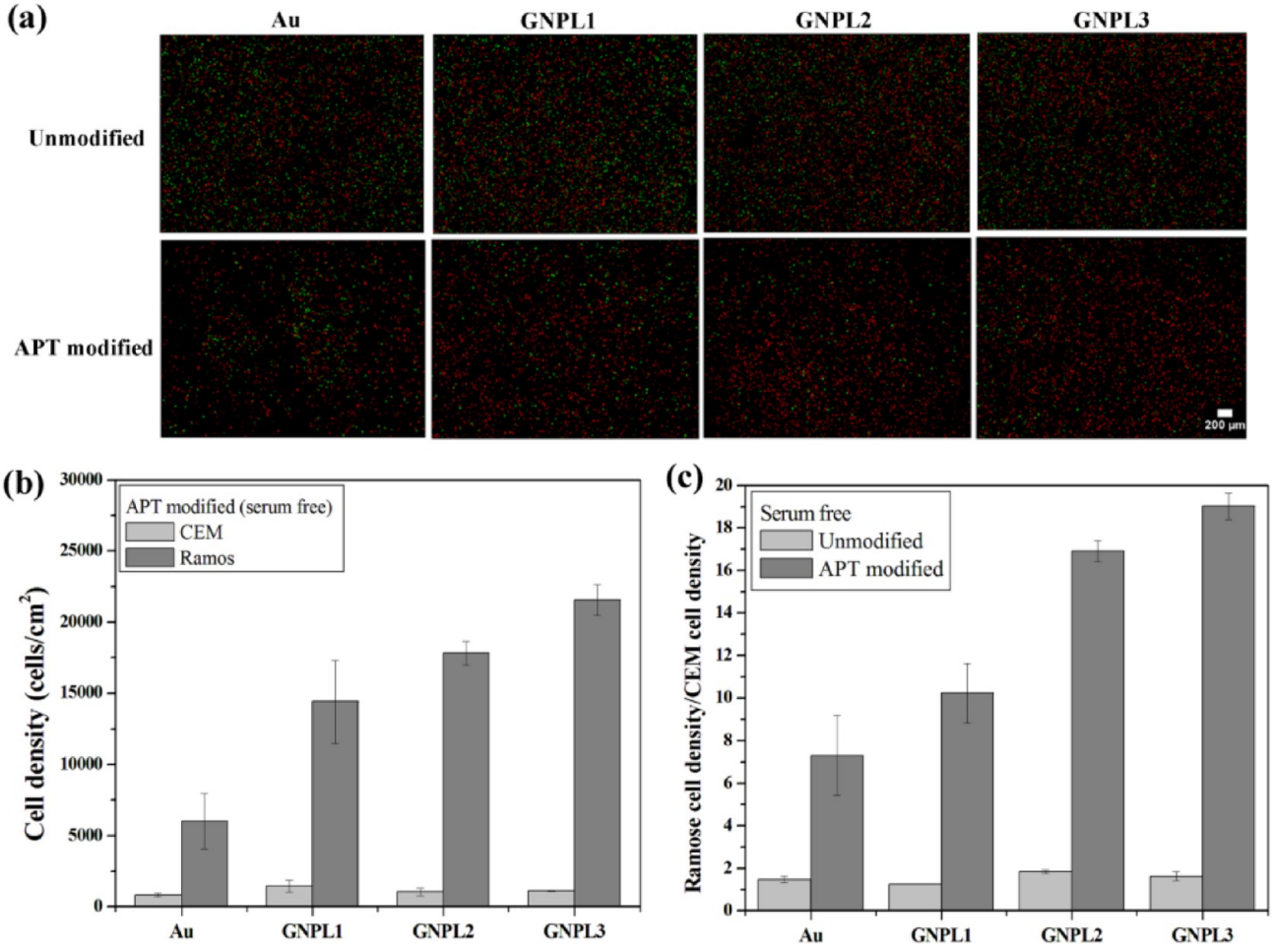

Figure 2. Selective capture of Ramos cells on Au-APT and GNPL(1 to 3)-APT surfaces in serum-free culture conditions. (a) Fluorescence images of Ramos (red) and CEM (green) on unmodified and APT-modified Au and GNPL(1 to 3) surfaces; (b) Ramos and CEM cell densities on Au-APT and GNPL(1 to 3)-APT surfaces (mean ± SD, n = 4); (c) ratio of Ramos and CEM cell densities on APT-modified and unmodified Au and GNPL(1 to 3) surfaces.

adhere to the GNPL surfaces (see Figure S1 in the Supporting Information). This behavior may be attributed to the micro/nano topographic structure of the GNPL surfaces. Cell interactions with this kind of material are effectively "three-dimensional", as opposed to "two-dimensional" in the case of smooth, planar surfaces. Interactions are thus expected to be more extensive and possibly stronger.

The selective capture of Ramos and CEM cells by APT-modified smooth gold and GNPL surfaces was then investigated. The two cell types were mixed in equal numbers and two groups of experiments were carried out, one group in a medium without serum and the other in a 10% serum medium. In serum-free conditions (Figure 2a), large numbers of Ramos cells (red) and CEM cells (green) adhered to the unmodified surfaces, and there was no significant difference in the cell densities. After aptamer modification of the smooth gold, the adhesion of CEM cells decreased. On the GNPL-APT surfaces the CEM cell density was also lower and decreased sharply as surface roughness increased. In contrast, Ramos cells adhered in large numbers on these surfaces. These data show that the GNPL-APT surfaces have good selectivity for Ramos cells in mixtures with CEM cells; the selectivity of the smooth surface modified using the same procedure was clearly lower than that of the nanoparticle layers.

To compare the selectivity of the surfaces for Ramos cells quantitatively, numerical adhesion densities were measured. Panels b and c in Figure 2 show the data for the serum-free group. On the unmodified Au and GNPL surfaces, the densities of Ramos and CEM cells were high, and the Ramos density was higher than the CEM (Figure S2a, Supporting Information). The densities of Ramos cells on the Au, GNPL1, GNPL2, and GNPL3 were, respectively, 1.5, 1.3, 1.9, and 1.6 times those of CEM cells (Figure 2c). This behavior may be attributed to the inherent adhesive properties of the Ramos cells: similar trends were observed in single cell systems. On the aptamer-modified surfaces, the CEM cell density decreased sharply (from ~14 000/cm^2 to ~1000/cm^2), whereas the density of Ramos cells remained high. On the aptamer-modified surfaces (Au and GNPL1 to 3), the Ramos cell densities were, respectively, 7.1, 10.2, 17.2, and 19.0 times those of CEM cells (Figure 2c). The selectivity of the aptamer-modified surfaces increased with increasing surface roughness, and the GNPL3-APT showed the highest selectivity for Ramos cells. It should be noted that the specific area of the GNPL surfaces increased with increasing surface roughness, implying increasing APT density; this may account for the increasing Ramos cell selectivity.

The cell interactions of the surfaces were also studied in a serum-containing medium as a more realistic environment. On the unmodified surfaces (Figure 3a), Ramos and CEM cell

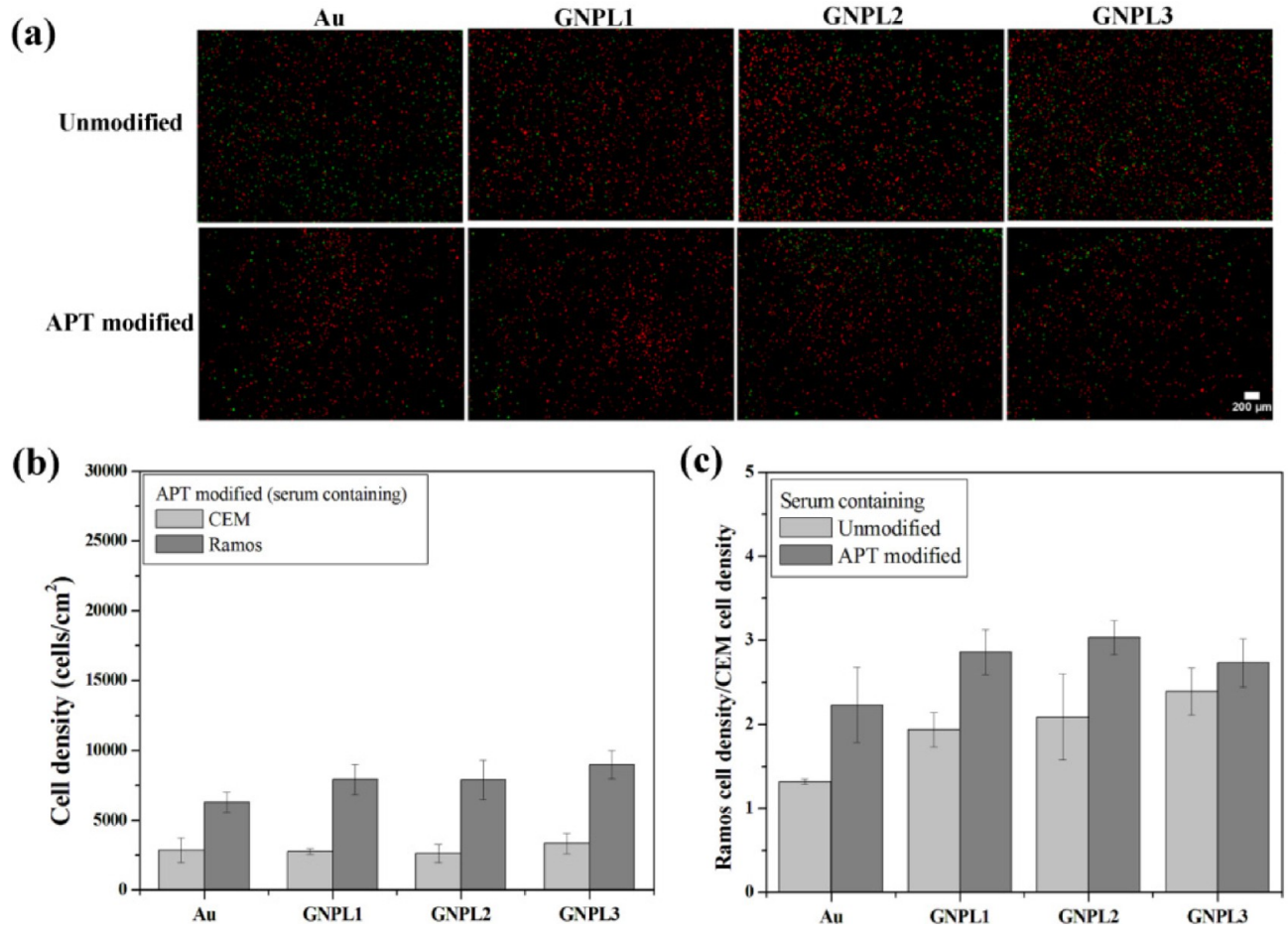

Figure 3. Selective capture of Ramos cells on Au-APT and GNPL(1 to 3)-APT surfaces in serum-containing culture conditions. (a) Fluorescence images of Ramos (red) and CEM (green) on unmodified and APT-modified Au and GNPL1 to 3 surfaces; (b) Ramos and CEM cell densities on Au-APT and GNPL(1 to 3)-APT surfaces (mean ± SD, n = 4); (c) ratio of Ramos to CEM cell densities on unmodified and APT-modified planar gold and GNPL1 to 3 surfaces.

densities in serum-containing conditions were significantly lower than in serum-free conditions (Figure 2a), and there was no significant difference in the densities of the two cell types. Similar to the serum-free group, the number of Ramos cells on the aptamer modified surfaces in serum-containing conditions increased with increasing surface roughness, but the cell density was lower, and the CEM cell number decreased more slowly with increasing surface roughness.

Panels b and c in Figure 3 show quantitative cell adhesion data for the unmodified and aptamer-modified surfaces in serum-containing conditions. The cell densities of Ramos on the smooth gold, GNPL1, GNPL2, and GNPL3 surfaces were, respectively, 1.3, 1.9, 1.9, and 2.2 times those of CEM cells (Figure 3c). In contrast, after aptamer modification, the proportion of Ramos cells increased significantly with increasing surface roughness and their densities on the smooth gold, GNPL1, GNPL2, and GNPL3 surfaces were, respectively, 2.2, 2.8, 3.0, and 2.7 times those of CEM cells. It may be concluded that in serum-containing conditions, the roughness of the GNPLs enhanced the selectivity of the aptamer for Ramos cells. However, compared with serum-free conditions, selectivity was much weaker.

Serum is highly complex, containing many types of protein. Proteins in the serum will adsorb nonspecifically and may "shield" the surface immobilized aptamer molecules to some extent, thus inhibiting binding of cell receptors to the immobilized aptamer, which we believe may be the main factor in the weakening of selectivity in serum compared to buffer.

Ramos Cell Capture on GNPL-POEGMA-APT. To improve the Ramos selectivity of the APT-modified surfaces in serum conditions, we introduced POEGMA as a protein resistant element.[22] POEGMA was attached by surface initiated ATRP and aptamer was then linked to the terminal hydroxyl groups of POEGMA by DSC activation to give Au-POEGMA-APT and GNPL-POEGMA-APT surfaces. Many studies have shown that the antifouling spacer influences the subsequent surface graft density of molecules or ligands.[26,27] Thus, we expect properties of the grafted POEGMA, such as its length, may influence the immobilization of aptamer on Au and GNPL surfaces. However, the performance of POEGMA as an antifouling spacer may also depend on its length. Considering these two aspects, we varied our experiment conditions and chose an optimal length of POEGMA of ~48 nm for the cell capturing assay.

In serum-free environment the cell densities were low on the POEGMA surfaces without aptamer (see Figure S3 in the Supporting Information). The adhesion numbers of Ramos and CEM cells were not different. Moreover, the cell densities did not change with surface roughness. After aptamer modification, the density of Ramos cells on the GNPL surfaces increased with increasing surface roughness, but the adhesion of both Ramos and CEM cells was still low, possibly because the micro/

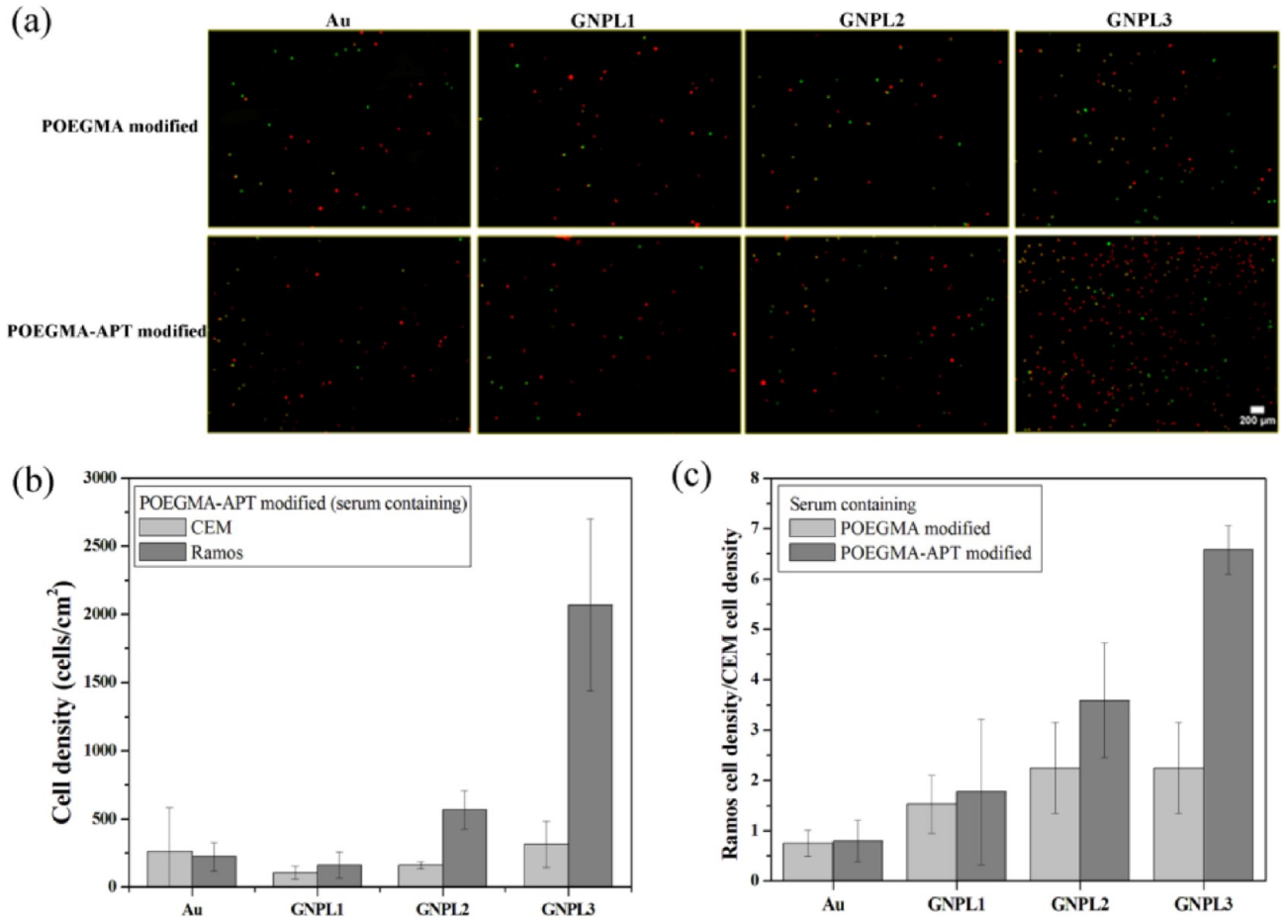

Figure 4. Selective capture of Ramos cells on Au-POEGMA-APT and GNPL (1 to 3)-POEGMA-APT surfaces in serum-containing conditions. (a) Fluorescence images of Ramos (red) and CEM (green) on unmodified (no APT) and APT-modified Au-POEGMA and GNPL(1 to 3)-POEGMA surfaces; (b) Ramos and CEM cell densities on Au-POEGMA-APT and GNPL (1 to 3)-POEGMA-APT surfaces (mean ± SD, n = 3); (c) ratio of Ramos to CEM cell densities on unmodified (no APT) and APT- modified Au-POEGMA and GNPL(1 to 3)-POEGMA surfaces.

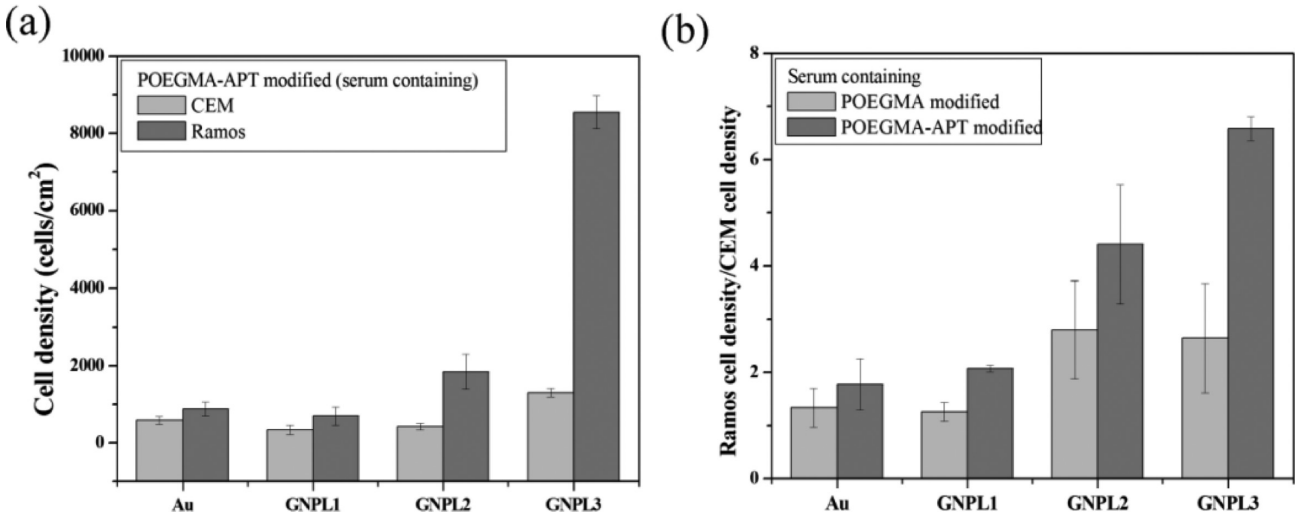

Figure 5. Selective capture of Ramos cells on Au-POEGMA-APT and GNPL (1 to 3)-POEGMA-APT surfaces in serum-containing conditions at 4 °C. (a) Ramos and CEM cell densities on Au-POEGMA-APT and GNPL (1 to 3)-POEGMA-APT surfaces (mean ± SD, n = 3); (b) ratio of Ramos to CEM cell densities on unmodified (no APT) and APT-modified Au-POEGMA and GNPL(1 to 3)-POEGMA surfaces.

nanotopographic structure enhanced the cell resistance of the POEGMA.

As shown in Figure 4a, in serum-containing conditions the numbers of cells on Au-POEGMA and GNPL(1 to 3)-POEGMA were clearly lower than those on Au-POEGMA-APT and GNPL(1 to 3)-POEGMA-APT. In addition, there was no observable difference in the numbers of Ramos and CEM cells. On the Au-POEGMA-APT and GNPL-POEGMA-

dx.doi.org/10.1021/am400469g | ACS Appl. Mater. Interfaces 2013, 5, 3816−3823

APT surfaces, there was no obvious difference in the number of CEM cells. However on the GNPL-POEGMA-APT, the number of Ramos cells increased with increasing surface roughness, indicating selectivity for Ramos cells. From these data, it may be concluded that in serum-containing environment, the GNPL-POEGMA-APT surfaces have good selectivity for Ramos cells in mixtures with CEM cells; the selectivity of the corresponding smooth gold surface is lower. The viability of the captured Ramos cells on Au-POEGMA-APT and GNPL-POEGMA-APT surfaces was measured using the MTT assay (Figure S5, Supporting Information). On the GNPL-POEGMA-APT, the absorbance values, both in single cell solution and binary cell mixtures, increased with increasing surface roughness, showing similar trends with cell number.

Panels b and c in Figure 4 show quantitative data for cell adhesion on the GNPL-POEGMA-APT surfaces in serum-containing conditions. The densities of both Ramos and CEM cells were relatively low on the surfaces without aptamer modification (Figure S4, Supporting Information): densities of Ramos cells on the four surfaces were, respectively, 0.8, 1.4, 2.2, and 2.1-fold those of CEM cells (Figure 4c). This trend was similar to that for the unmodified GNPLs (Figure 3c). After modification of POEGMA by aptamer, the density of Ramos cells increased significantly, whereas the density of CEM cells did not change. The densities of Ramos cells on the four POEGMA surfaces modified with aptamer were, respectively, 0.9, 1.5, 3.5, and 6.6 times those of CEM (Figure 4c), indicating that the selectivity of GNPL-POEGMA-APT for Ramos cells was significantly enhanced with increase in surface roughness. This effect may be attributed to the protein resistance of the POEGMA, excluding the surface proteins that might "shield" the immobilized aptamer.

All the Ramos cell capture assays mentioned above were performed at 37 °C. However, since aptamer TD05 was selected at 4 °C and showed a higher binding affinity for Ramos cell than that at 37 °C, cell capture assays have also been performed at 4 °C.[28,29] To see whether the temperature of the cell capture assay plays a role to the selectivity for Ramos cell, we also performed Ramos cell capture assays on GNPL-POEGMA-APT surfaces at 4 °C. As shown in Figure 5, although the selectivity of Ramos made no significant change, indicating that temperature has little influence on selectivity of aptamer TD05 in this work, the capture efficiency of GNPL-POEGMA-APT surfaces was greatly improved at 4 °C.

CONCLUSIONS

Micro/nanostructured gold nanoparticle layers with varying surface roughness were modified with TD05 aptamer. In mixtures of Ramos and CEM cells under serum-free conditions, the density of Ramos cells on the roughest GNPL surface was 19 times that of CEM. However, the selectivity of GNPL-APT surfaces was much less in serum-containing conditions. GNPL-POEGMA-APT surfaces with POEGMA as an antifouling spacer, showed good selectivity for Ramos cells in serum-containing medium, and selectivity increased with increasing surface roughness. The density of Ramos cells was 6.6 times that of CEM cells on the roughest (GNPL3-POEGMA-APT) surface. The data generated in this study suggest that surfaces combining appropriate chemical composition and micro/nano topographic structure may be useful for cell separation, including the isolation of cancer cells for diagnosis.

ASSOCIATED CONTENT

Supporting Information

Fluorescence images of Ramos and CEM on unmodified Au and GNPL(1 to 3) surfaces in single cell solutions; Ramos and CEM cell densities on Au and GNPL(1 to 3) surfaces in binary cell mixtures; fluorescence images of Ramos and CEM on unmodified (no APT) and APT-modified Au-POEGMA and GNPL(1 to 3)-POEGMA surfaces (serum free); Ramos and CEM cell densities on Au-POEGMA and GNPL(1 to 3)-POEGMA surfaces (serum containing). This material is available free of charge via the Internet at http://pubs.acs.org.

AUTHOR INFORMATION

Corresponding Author

*Tel: +86-512-65880827. Fax: +86-512-65880583. E-mail: liuxiaoli@suda.edu.cn (X.L.); chenh@suda.edu.cn (H.C.).

Notes

The authors declare no competing financial interest.

ACKNOWLEDGMENTS

This work was supported by the National Science Fund for Distinguished Young Scholars (21125418) and the Priority Academic Program Development of Jiangsu Higher Education Institutions (PAPD). The authors thank Dr. John L. Brash of McMaster University for helpful discussions.

REFERENCES

(1) Choi, Y. E.; Kwak, J. W.; Park, J. W. *Sensors* **2010**, *10*, 428−455.
(2) Clare, S. E.; Sener, S. F.; Wilkens, W.; Goldschmidt, R.; Merkel, D.; Winchester, D. J. *Ann. Surg. Oncol.* **1997**, *4*, 447−451.
(3) Braun, S.; Pantel, K.; Muller, P.; Janni, W.; Hepp, F.; Kentenich, C. R. M.; Gastroph, S.; Wischnik, A.; Dimpfl, T.; Kindermann, G.; Riethmuller, G.; Schlimok, G. *N. Engl. J. Med.* **2000**, *342*, 525−533.
(4) Alunni-Fabbroni, M.; Sandri, M. T. *Methods* **2010**, *50*, 289−297.
(5) Gertler, R.; Rosenberg, R.; Fuehrer, K.; Dahm, M.; Nekarda, H.; Siewert, J. *Recent Results Cancer Res.* **2003**, *162*, 149−156.
(6) Zigeuner, R. E.; Riesenberg, R.; Pohla, H.; Hofstetter, A.; Oberneder, R. *J. Urology* **2003**, *169*, 701−705.
(7) Vona, G.; Sabile, A.; Louha, M.; Sitruk, V.; Romana, S.; Schütze, K.; Capron, F.; Franco, D.; Pazzagli, M.; Vekemans, M. *Am. J. Pathol.* **2000**, *156*, 57−63.
(8) Müller, V.; Stahmann, N.; Riethdorf, S.; Rau, T.; Zabel, T.; Goetz, A.; Jänicke, F.; Pantel, K. *Clin. Cancer Res.* **2005**, *11*, 3678−3685.
(9) Pantel, K.; Alix-Panabieres, C.; Riethdorf, S. *Nat. Rev. Clin. Oncol.* **2009**, *6*, 339−351.
(10) Thiery, J. P.; Sleeman, J. P. *Nat. Rev. Mol. Cell Biol.* **2006**, *7*, 131−142.
(11) Yang, J.; Weinberg, R. A. *Dev. Cell* **2008**, *14*, 818−829.
(12) Ranella, A.; Barberoglou, M.; Bakogianni, S.; Fotakis, C.; Stratakis, E. *Acta Biomater* **2010**, *6*, 2711−2720.
(13) Fischer, K. E.; Alemán, B. J.; Tao, S. L.; Daniels, R. H.; Li, E. M.; Bünger, M. D.; Nagaraj, G.; Singh, P.; Zettl, A.; Desai, T. A. *Nano Lett.* **2009**, *9*, 716−720.
(14) Proske, D.; Blank, M.; Buhmann, R.; Resch, A. *Appl. Microbiol. Biotechnol.* **2005**, *69*, 367−374.
(15) Fichou, Y.; Ferec, C. *Trends Biotechnol.* **2006**, *24*, 563−570.
(16) Ulrich, H.; Trujillo, C. A.; Nery, A. A.; Alves, J. M.; Majumder, P.; Resende, R. R.; Martins, A. H. *Comb. Chem. High Throughput Screening* **2006**, *9*, 619−632.
(17) Kanwar, J. R.; Roy, K.; Kanwar, R. K. *Crit. Rev. Biochem. Mol. Biol.* **2011**, *46*, 459−477.
(18) Medley, C. D.; Bamrungsap, S.; Tan, W.; Smith, J. E. *Anal. Chem.* **2011**, *83*, 727−734.
(19) Chen, L.; Liu, X.; Su, B.; Li, J.; Jiang, L.; Han, D.; Wang, S. *Adv. Mater.* **2011**, *23*, 4376−4380.

(20) Zhou, Q.; Liu, Y.; Shin, D. S.; Silangcruz, J.; Tuleuova, N.; Revzin, A. *Langmuir* **2012**, *28*, 12544−12549.
(21) Wan, Y.; Mahmood, M. A.; Li, N.; Allen, P. B.; Kim, Y. T.; Bachoo, R.; Ellington, A. D.; Iqbal, S. M. *Cancer* **2012**, *118*, 1145−1154.
(22) Zhou, F.; Li, D.; Wu, Z.; Song, B.; Yuan, L.; Chen, H. *Macromol. Biosci.* **2012**, *12*, 1391−1400.
(23) Montagne, F.; Polesel-Maris, J.; Pugin, R.; Heinzelmann, H. *Langmuir* **2008**, *25*, 983−991.
(24) Ma, H.; Li, D.; Sheng, X.; Zhao, B.; Chilkoti, A. *Langmuir* **2006**, *22*, 3751−3756.
(25) Wenzel, R. N. *Ind. Eng. Chem.* **1936**, *28*, 988−994.
(26) Yu, Q.; Zhang, Y.; Wang, H.; Brash, J.; Chen, H. *Acta Biomater.* **2011**, *7*, 1550−1557.
(27) Li, D.; Chen, H.; Brash, J. L. *Colloids Surf., B* **2011**, *86*, 1−6.
(28) Zhou, J.; Soontornworajit, B.; Wang, Y. *Biomacromolecules* **2010**, *11*, 2087−2093.
(29) Wu, Y.; Sefah, K.; Liu, H.; Wang, R.; Tan, W. *Proc. Natl. Acad. Sci. U.S.A.* **2010**, *107*, 5−10.